DESIGN OF HIGHER BANDWIDTH MODEL FOLLOWING FOR FLIGHT VEHICLE STABILIZATION AND CONTROL

Frohmut Henschel and Gerhard Bouwer
Deutsche Forschungs- und Versuchsanstalt
für Luft- und Raumfahrt e.V.,
Institut für Flugmechanik, Braunschweig

Abstract

The paper describes the general design of a Model Following Control System (MFCS), which is accomplished in several sequential steps. To start with, a suitable structure for the controller is chosen depending on the physical properties of the system and operating constraints. The feedforward gains are determined by calculating a pseudoinverse of the control input matrix assuming the plant to be linear. The feedback gains are obtained by using an interactive vector performance optimization technique. The desired design goals are achieved by selecting a proper set of performance criteria in the time and frequency domain. The design obtained by this procedure is tested extensively using offline and ground based nonlinear and real-time simulation facilities.

The approach is applied both to the fixed wing and helicopter inflight simulators ATTAS (VFW 614) and ATTHeS (BO 105) at DFVLR. Simulation results demonstrate the effectiveness of the MFCS in obtaining good model matching and desired disturbance rejection with good crossover properties.

Nomenclature

A	system dynamics matrix
B	control input Matrix
C	output matrix
D	damping
$G(s)$	transfer function matrix
J_i	elements of the performance index vector
I	identity matrix
K	feedback gain matrix
L	number of PIV elements (11)
$L(s)$	Lagrangean function (appendix)
$V(k)$	performance index
c_i	elements of the weighting vector
e	model following error vector
$g_v^T(s)$	v-th row vector in the transfer function matrix
h	Euclidean norm of an output vector (appendix)
n	dimension in the state vector
m	dimension in the control vector
q	pitch rate
s	Laplace variable ($j\omega$)
t	time
u	control input vector
$\bar{u}$	feedback control vector
x	state vector
α	real part of the input vector (appendix)
β	imaginary part of the input vector (appendix)
β	side slip angle
δ_a	aileron position
δ_{DLC}	direct lift control flap position
δ_{el}	elevator position
δ_{tr}	pedal position
δ_r	rudder position
δ_{th}	throttle position
δ_x	longitudinal stick position
δ_y	lateral stick position
δ_0	collective control position
λ^2	Lagrangean multiplier (appendix)
ρ	spread factor
$\overline{\sigma}$	maximum singular values
$\underline{\sigma}$	minimum singular values
σ_{dv}	individual singular values (output disturbance)
σ_{sv}	individual singular values (sensor noise)
ω	angular frequency in radians/second

Subscripts

f	feedforward
m	model
max	value for maximum
min	value for minimum
o	output
v	v-th row vector

Superscripts

T	transpose of a matrix
$+$	pseudoinverse of a matrix
-1	inverse of a square matrix
$\cdot$	time derivative
$-$	conjugate complex value

I. Structure of Model Following Control System

A model following control system (MFCS), shown in Figure 1, as a special type of control system, which forces an existing plant (host aircraft) to behave like a given model [3] , [5] .

General Structure:

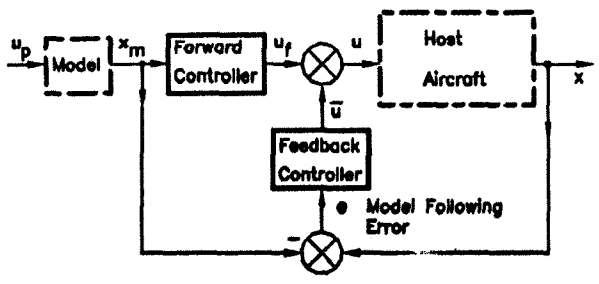

Figure 1. Principle of explicit model following

The model states x_m are controlled by the pilot inputs u_p. A forward controller approximates the model following by generating control inputs u_f to the plant.

The feedback controller generates additional controls $\bar{u}$ out of the model following error e to suppress inaccuracies and disturbances.

Let the plant be described by

$$\begin{aligned} \dot{x} &= A \cdot x + B \cdot u \\ y &= C \cdot x \quad (C = I) \end{aligned} \tag{1}$$

and the model

$$\dot{x}_M = A_M \cdot x_M + B_M \cdot u_p. \tag{2}$$

In the first step the forward controller is defined to achieve model following. With $x \equiv x_M$ the forward controls are

$$u_f = B^+ \cdot (\dot{x}_M - A \cdot x_M) \tag{3}$$

with B^+ as the pseudoinverse of B.

The model following error

$$e = x - x_M \tag{4}$$

can be written as (2) - (1) = (3)

$$\begin{aligned} \dot{e} = A \cdot e + (I - B \cdot B^+) \cdot (\dot{x}_M - A \cdot x_M) \\ + B \cdot \bar{u}. \end{aligned} \tag{5}$$

If n = m , i.e. the number of controls m is equal to the number of states n , $I - B \cdot B^+ = 0$ and with the initial conditions $x_0 = x_{M0}$ and e = 0 , follows $\bar{u} \equiv 0$ and $e \equiv 0$. In this case, perfect model following is obtainable.

If $n > m$ and $\bar{u} \not\equiv 0$, then $I - B \cdot B^+ \neq O$ and from eq.5 it can be seen, that the error dynamic has the system dynamic and even may have constant terms from $(I - B \cdot B^+) \cdot (\dot{x}_M - A \cdot x_M)$.

Therefore, a proportional and integral controller is necessary to influence the error dynamic and suppress constant errors. In addition, the controller has to reduce the influences of disturbances.

These disturbances can be divided in

1) output disturbances (gust, plant nonlinearities, uncertainties and parameter changes due to changes in flight condition and mass).

and

2) sensor noise.

The dynamics of the disturbances, shown in Figure 2 are totally different. The overall input-output behaviour can be written as

$$\begin{aligned} x = (I - G \cdot K)^{-1} G \cdot K \cdot (r + \eta) \\ + (I - G \cdot K)^{-1} d \end{aligned} \tag{6}$$

To suppress the output disturbances and to achieve high performance, with

$$\lim_{\|K\| \to \infty} \|(I - G \cdot K)^{-1}\| = 0 \tag{7}$$

the controller has to be of infinitive gain.

In this case, the sensor noise

$$\lim_{\|K\| \to \infty} \|(I - G \cdot K)^{-1} G \cdot K\| = 1, \tag{8}$$

is directly transferred to the system.

To suppress sensor noise, the controller has to be zero, because

$$\lim_{\|K\| \to 0} \|(I - G \cdot K)^{-1} G \cdot K\| = 0, \tag{9}$$

but with

$$\lim_{\|K\| \to 0} \|(I - G \cdot K)^{-1}\| = 1 \tag{10}$$

there is a direct transfer of output disturbance which leads to low performance of the system.

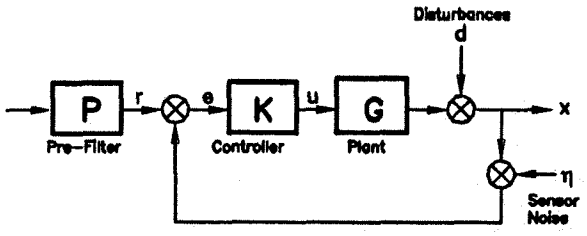

Figure 2. Disturbances

Between these opposite conditions, an acceptable compromise has to be found with the feedback controller layout procedure.

II. Physical Constraints of the Plant to be Controlled

Before starting any layout procedure for the feedback control system, the physical constraints of the plant have to be considered carefully. Since the layout procedure, described in this paper is applied to both VFW 614 ATTAS and Bo 105-S ATTHeS, the main differences for controller layout between these vehicles are described.

First the dynamics of the uncontrolled systems has to be analysed. For both vehicles the natural frequencies and damping of the typical oscillations is listed in Table 1 (frequencies in rad/sec). It can be seen, that the quick motions of the helicopter respond four-times faster than these modes of the fixed wing.

In addition, the phygoid mode of the helicopter is unstable.

Furthermore, some properties of the plant, such as couplings, additional degrees of freedom and the type of disturbances as listed in Table 2 influence the layout procedure. The decoupled longitudinal/lateral motions of the fixed wing make possible a seperate controller layout for each of these motions, whereas the layout for the helicopter controllers has to be achieved in one step for all axes.

The additional degrees of freedom (Table 2) can be neglected in the fixed wing-layout, but are of severe influence in the helicopter control system layout. In addition the rotor vibrations are in the same frequency range as the controlled plant and thus require a carefully layout of filters in the measurement system.

	ATTAS 125 kts	ATTHeS 60 kts
Phygoid	$\omega_0 = 0.203$ $D = 0.068$	$\omega_0 = 0.32$ $D = -0.017$
Short Period	$\omega_0 = 1.61$ $D = 0.58$	$\omega_0 = 5.2$ $D = 1.0$
Dutch Roll	$\omega_0 = 1.05$ $D = 0.26$	$\omega_0 = 2.4$ $D = 0.25$
Roll Time Constant	$T_R = 0.625\ s$	$T_R = 0.11\ s$
Spiral Mode	$T_S = -41.9\ s$	$T_S = 18.8\ s$

Table 1. Comparison of natural modes ATTAS - ATTHeS

	ATTAS	ATTHeS
Couplings	longitudinal /lateral decoupled	between all states
Additional degrees of freed om	Structural modes $\omega \approx 5$ 1/s	Rotor flapping $\omega \approx 53$ 1/s
disturbances	gust	gust, Rotor vibrations $\omega \approx 44$ 1/s

Table 2. Couplings and disturbances

Due to these differences between fixed wing and helicopter application, the layout procedures are different for these systems.

The controller layout for the fixed wing can be performed in two independant steps for the longitudinal and lateral axes. The necessary feedbacks are listed in Table 3.

**	u	α	q	Θ	∫u	∫α	∫Θ	r	p	β	Φ	∫β
δ_{el}	0	0	X	X	0	0	X	0	0	0	0	0
δ_{DLC}	0	X	0	0	0	X	0	0	0	0	0	0
δ_{th}	X	0	0	0	X	0	0	0	0	0	0	0
δ_a	0	0	0	0	0	0	0	0	X	X	X	0
δ_r	0	0	0	0	0	0	0	X	0	X	0	X

Table 3. Active loops (fixed wing)

**	u	α	q	Θ	∫α	∫Θ	r	p	Φ	∫r	∫Φ
δ_x	0	X	X	X	X	X	0	X	X	0	X
δ_Φ	0	X	X	X	X	X	0	0	0	0	X
δ_y	0	0	X	0	0	0	0	X	X	0	X
δ_{tr}	0	X	X	X	X	X	X	0	0	X	0

Table 4. Active loops (helicopter)

Due to the decoupled modes, no feedbacks between longitudinal and lateral motions are necessary, which can be seen in the upper right and lower left part of the feedback-matrix.

The helicopter control system layout [1] has to be performed in one step. The necessary feedbacks are listed in Table 4 In comparison with Table 3 the strong coupling of the systen leads to 12 more feedback loops and thus 12 more feedback gains to be optimized.

III. Feedback Controller Layout

The feedback gains of the model following system are selected to minimize the sensitivity of the controlled system to variations in plant parameters and external disturbances. These gains are obtained by using a computer aided design technique based on Kreisselmeier's vector performance optimization [4] .

In order to apply the above technique, each design objective is formulated quantitatively in terms of a performance criterion. The criterion is selected such that its minimization results in improvement in the performance. The final design compromise is obtained by systematically minimizing the following cost function in several steps

$$V(k) = \min_k \left\{ \frac{1}{\rho} \cdot \ln \sum_{i=1}^{L} \left[\exp\left(\frac{J_i(k)}{c_i} \right) \right]^{\rho} \right\} \qquad (11)$$

where $\rho = 20$ and c_i the elements of the weighting vector is selected such that $J_i/c_i \leq 1$. The weights c_i are selected to make J_i/c_i approximately 1, 0.7 or 0.5 depending on whether the corresponding elements J_i are to be further minimized, retained at the same value or can be allowed to increase.

The different performance criteria used for the longitudinal axes of a fixed wing are dicussed in the following.

The first set of four criteria are output time responses of the controlled aircraft excited by a high bandwidth + constant (3-2-1-1 + DC) input. The input is a series of four continuous steps with alternating signs, lasting for 3, 2, 1, 1 time units. The length of the time unit can be adjusted to centre the frequency band of the input around the system natural frequencies. These measures are computed as a summation over a time interval T_0 to T_f by using a discrete time equivalent of the equations given below.

$$J_i = \int_{T_0}^{T_f} e^{at} \cdot |x_i(t)| \cdot dt \qquad (a \geq o\ ,\ i = 1,2,3,4) \qquad (12)$$

The choice of T_f govern how fast the responses decay and the location of the closed loop poles. Rate/position limits time delays and hysteresis of the actuators are included in the computations of the time responses.

The second set of eight criteria is derived from singular value decomposition of the appropriate transfer function matrices. The measures are primarily used to constrain the feedback gains and to minimize the effect of high frequency sensor noise. Hence the the transfer function

matrices for both sensor noise and output disturbances are considered for optimization.

Minimization of output disturbances can be obtained only at the expense of sensor noise and hence the desired compromise is dependant on the noise characteristics of the individual sensors. To obtain more flexibility during minimization modified measures called individual singular values (ISV) are computed. The criteria given in Equations (13) ,(14) are derived in the appendix.

$$J_{4+i} = \max_{\omega} \bar{\sigma}_{d_i} \{[\, I - G(j\omega)K \,]^{-1}\} \tag{13}$$

$$J_{8+i} = \max_{\omega} \bar{\sigma}_{s_i} \{[\, I - G(j\omega)K \,]^{-1} G(j\omega)K \} \tag{14}$$

$\bar{\sigma}_{di}, \bar{\sigma}_{si}$ are the maximum ISV for output disturbances and sensor noise respectively and are selected over a frequency range of $\omega_l = 2$ to $\omega_h = 30$ radians per second. These measures are found to be more flexible and effective in limiting the feedback gains than direct gain constraints.

To minimize the sensitivity of the controlled system to variation in the plant parameters caused by changes in flight condition, criteria $J_{1,2,3,4}$ are calculated at two additional flight conditions. These conditions are selected to give a maximum variation in dynamic pressure within the "island of operation" for example, low attitude, low speed flight conditions. Thus maximum of $3 \cdot 4 + 8 = 20$ criteria need to be considered for designing the feedback gains.

IV. Simulation Results

The obtained MFCS-parameters were implemented on nonlinear, generic programs of ATTAS and ATTHeS, including simulation of actuating systems, sensors, data aquisition systems, measurement noise. The explicit models to be followed were represented by a linear, 6 DOF model of an Airbus-type transport aircraft for the ATTAS MFCS and a model of the BK117-type helicopter for the ATTHeS MFCS. In addittion, a gust simulation procedure was available for the ATTAS simulation model.

Both ATTAS and ATTHeS MFCS performance are investigated with 3-2-1-1 longitudinal control inputs to the models to be followed. Figure 4 shows the 0.1 mm elevator (XCHP) input to the model and the control system activity in elevator (ETA), direct lift flaps (ETADLC) and thrust (SCHUBL) to the ATTAS model. The commanded model response in airspeed (UM), angle of attack (ALFAM), and pitch rate (QM) and the corresponding ATTAS response is shown in Figure 5.

It can be seen, that the gust rejection is namely done by the elevator activities. The gust velocities in longitudinal (UTURB), lateral (VTURB), and vertical (WTURB) directions are shown in Figure 6. Especially the turbulence (QTURB) as is shown in Figure 7 at t=17 sec disturbes the ATTAS angle of attack and pitch rate, but is very well suppressed by the elevator control.

The ATTHeS control activity longitudinal (DX), lateral (DY), vertical (DC) and directional (DH) axes is shown in Figure 8 for the input to the BK117-type model in the dashed lines and for the control system in the solid lines. Because the ATTHeS couplings, the activities of all controls is of the same size to achieve the model following. Figure 9 describes the system response in pitch (Q), roll (P) , and yaw (R) rate and angle of attack (ALFA) for the model (-COM) and ATTHeS (-GER).

It can be seen, that especially in the yaw rate and the angle of attack a very good model following is achieved. The delay of about 100 milliseconds in pith and roll rate is caused by the delay of the actuating system (40 ms) and the rotor system (30 ms).

V. Conclusions

The layout procedure for a Model Following Control system is presented. The feed-forward controllers are calculated simply by inverting the plant dynamics. To suppress the influence of changes and incertainities in plant parameters and gust, proportional and integral feedback controllers are necessary. Since these controllers implement additional sensor noise to the controlled system, a compromise is to be found for the layout. The physical constraints of the plant have to be carefully considered to achieve an optimum performance with a minimum of feedback gains. The main difference between MFCS layout for fixed wing and helicopter is the strong coupling of the helicopter, which leads to a much complexer control system.

The layout procedure minimizes a large number of performance criteria by an optimization procedure.

The nonlinear simulation results of both fixed wing Figure 5 and helicopter MFCS Figure 9 application demonstrate a high efficiency of the systems in model following as well as in disturbance rejection.

Appendix

Individual Singular Values.

Let

$$x_0 = G(s) \cdot u \tag{15}$$

where $G(s)$ is the transfer function matrix between the n outputs x_0 and m inputs u .

$$G(s) = (sI - A)^{-1} B \tag{16}$$

The use of spectral norms as measure of matrix size has led to singular value decomposition being used to characterize performance/stability robustness of MIMO systems.

By definition

$$\sigma_{max} = \bar{\sigma} = \sqrt{\lambda^2_{max}}$$
$$\sigma_{min} = \underline{\sigma} = \sqrt{\lambda^2_{min}} \tag{17}$$

where $\lambda^2_{max}, \lambda^2_{min}$ are the maximum and minimum eigenvalues of the positive semidefinite Hermitian matrix [2]

$$G^T(-j\omega) \cdot G(j\omega) \tag{18}$$

$\bar{\sigma}, \underline{\sigma}$ is the maximum (minimum) output gain for all possible normalized input combinations, the output and input expressed as Euclidean n[illegible] The related eigen-

vector gives the amplitude and phase of the input component which generates this maximum (minimum). To obtain effective measure of performance which can be used directly for optimization, the theory is extended to each output variable i.e. the system is split into n single-output multi-input systems:

$$x_{0,\nu} = g_\nu^T(s) \cdot u \tag{19}$$

where $x_{0,\nu}$ is the *vth* element of the output vector and g_ν^T is the *vth* row of the transfer function matrix.

For a given normalized input

$$\bar{u}^T \cdot u = (\alpha - j\beta)^T \cdot (\alpha + j\beta) = 1 \tag{20}$$

one can obtain the corresponding output

$$h_\nu^2 = (\alpha - j\beta)^T \cdot [\, g_\nu(-j\omega) \cdot g_\nu^T(j\omega)] \cdot (\alpha + j\beta).$$

Construct a Lagrangean Function $L(\omega)$ with a factor λ_ν^2.

$$L(\omega) = h_\nu^2 - \lambda_\nu^2 \cdot (\bar{u}^T \cdot u - 1).$$

To get the maximum of $L(\omega)$ the gradient of L with respect to all components α_ν, β_ν must be made equal to zero i.e.

$$[g_\nu(-j\omega) \cdot g_\nu^T(j\omega)] \cdot (\alpha + j\beta) - \lambda_\nu^2 \cdot (\alpha + j\beta) \stackrel{!}{=} 0.$$

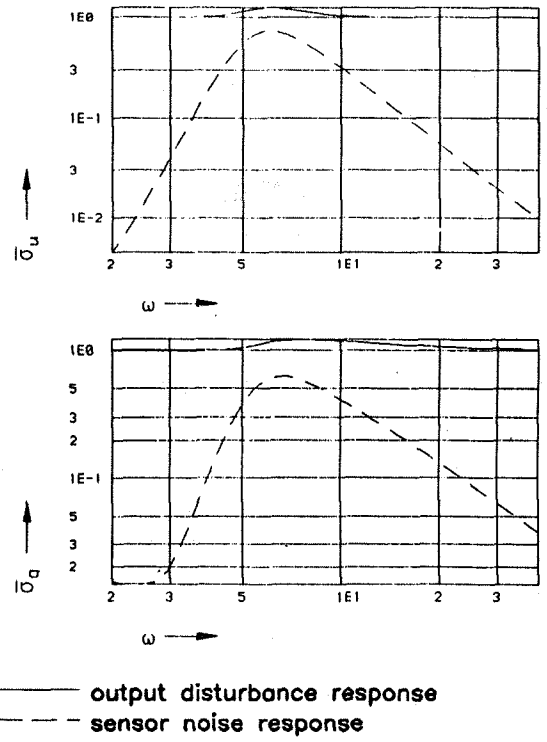

Figure 3. Two typical individual singular value plots for fixed wing.

The range of $\bar{g}_\nu \cdot g_\nu^T$ is one of and because the matrix is positive-definite there exists $\lambda_\nu = \lambda_{\nu\,max} > 0$. And hence

$$h_{\nu\,max} = \lambda_{\nu\,max}(\omega) \tag{20}$$

$h_{\nu\,max}$ is the maximum output ampitude of the *vth* variable for all possible normalized input combination of amplitude and phase for a given frequency ω.

One can obtain individual $\lambda_{\nu\,max}$ for all outputs over a frequency range of interrest and use these as measure of disturbance suppression in each variable $x_{0,\nu}$.

By choosing the appropriate transfer functions depending on where the noise/disturbance enters the system, one can obtain several measures. Figure 3 shows typical ISV plots for pitch rate (q) and forward velocity (u) obtained after optimization procedure.

Bibliography

[1] Bouwer, G. *Design on Flight Testing of a Model Following Control System for Helicopter.* IFAC-Congress, Vol.6, July 1987, pp 118-124.

[2] Doyle, J.C. and Stein, G. *Multivariable Feedback Design: Concepts for Classical/Modern Synthesis.* IEEE-Transaction on Automatic Control, Vol. AC-26, No.1, Febr. 1981.

[3] Henschel, F. *On Control Concepts for In Flight Simulation Including Actuator Nonlinearities and Time Delays.* ESA-TT-948, 1985.

[4] Kreisselmeier, G. and Steinhauser, R. *Systematic Control Design by Optimizing a Vector Performance Index.* IFAC-Symposium on Computer Aided Design of Control Systems, Aug.1979, pp.113-117.

[5] Motyka, P.R., Rynaski, E.G. and Reynolds, P.A. *Theory and Flight Verification of the TIFS Model Following System.* Journal of Aircraft, Vol.9, No.5, May 1972.

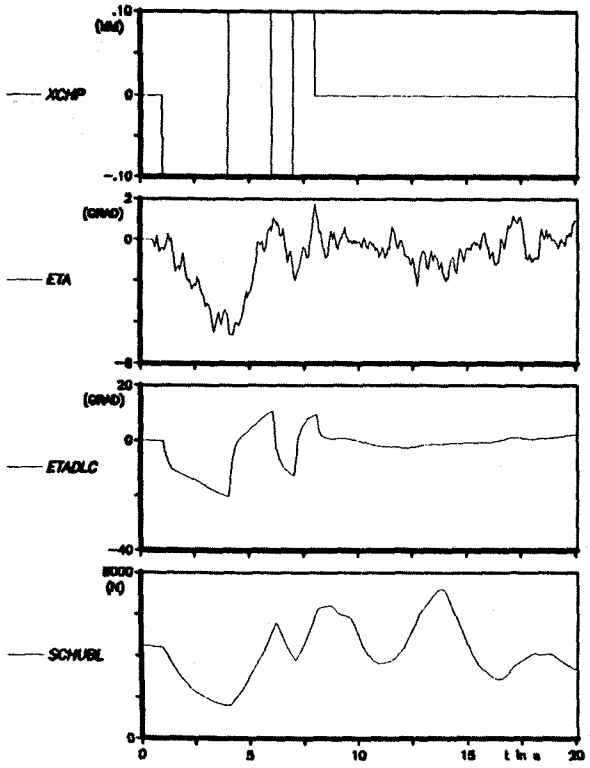

Figure 4. Controller activities for ATTAS MFCS.

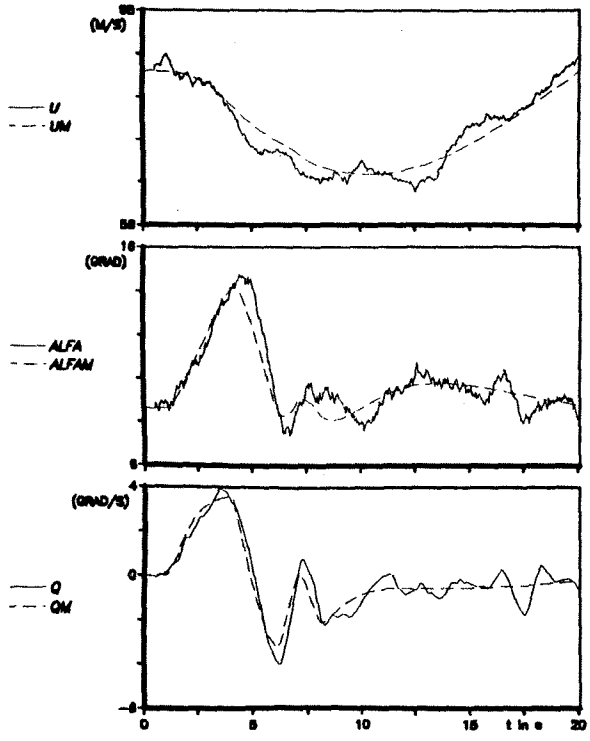

Figure 5. Model matching and disturbance rejection for ATTAS MFCS.

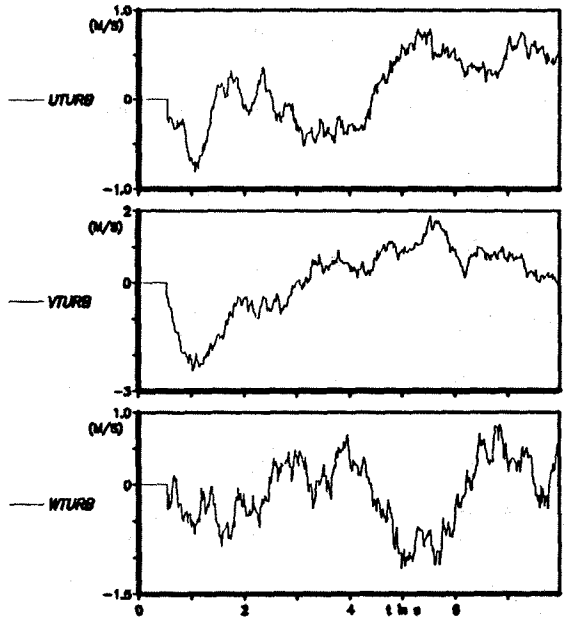

Figure 6. Calculated gust velocities fed into ATTAS MFCS.

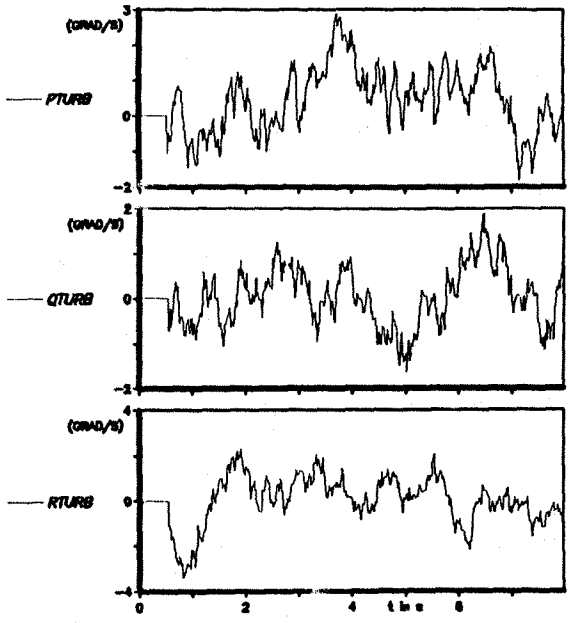

Figure 7. Calculated turbulences fed into ATTAS MFCS.

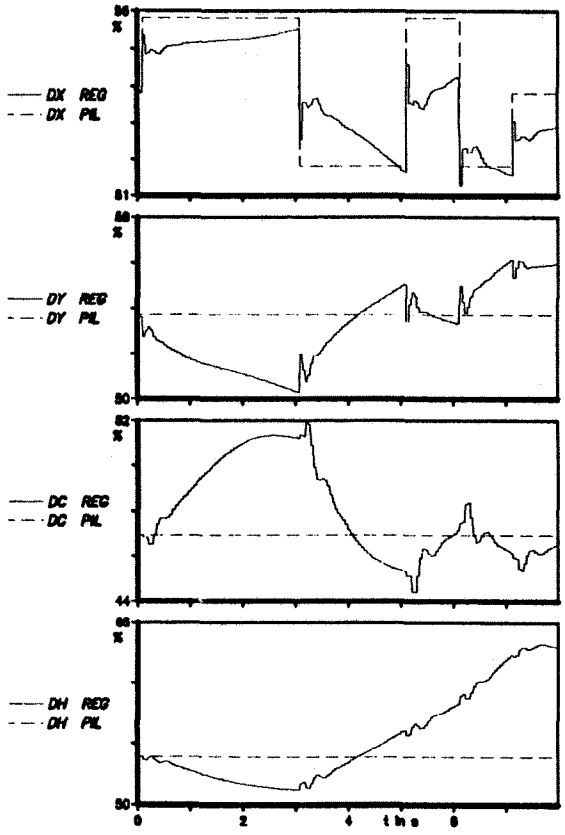

Figure 8. Controller activities for ATTHeS MFCS.

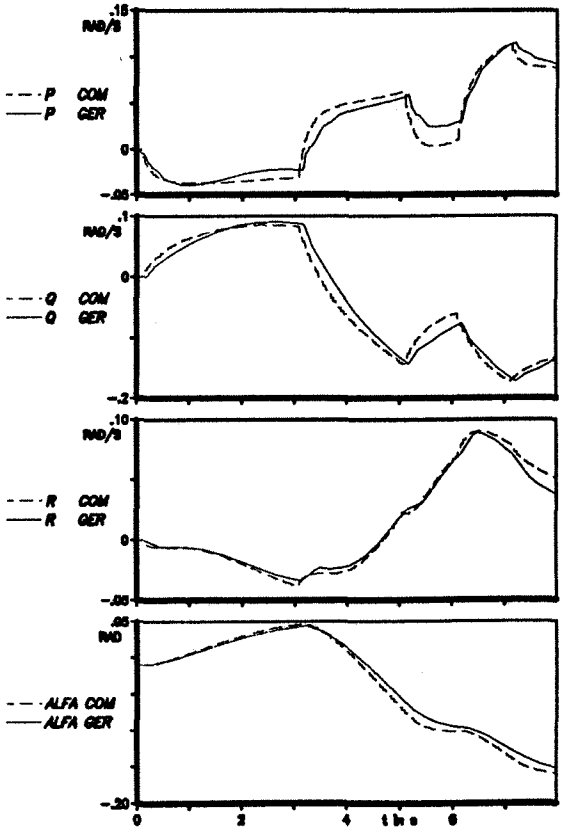

Figure 9. Model matching for ATTHeS MFCS.